Mechanics Research Communications 132 (2023) 104165

Contents lists available at ScienceDirect

Mechanics Research Communications

journal homepage: www.elsevier.com/locate/mechrescom

Shape optimization of non-rigid origami leading to emerging bistability ☆

Yibo Wang, Ke Liu *

Department of Advanced Manufacturing and Robotics, Peking University, Beijing, 100871, China

ARTICLE INFO

Keywords:
Origami
Nonlinear mechanics
Shape optimization
Bifurcation theory
Large deformation

ABSTRACT

Origami structures are a type of thin-walled flexible structures that undergo large deformation. Their inherent non-rigid characteristic empowers them with great potential for applications in space structures, metamaterials, and robotics. To understand the large deformation of origami structures, consideration of nonlinear mechanics is necessary. However, most origami structures are still designed by pure geometric approaches without considering their non-rigid behavior. In this work, we propose a computational design framework that incorporates nonlinear mechanics into the design procedure of origami. Guided by minimization of stored energy, under prescribed displacement boundary conditions, we optimize the configuration of origami structures. Difficulties arise due to the complex energy landscape of origami structures that inevitably induces bifurcation. We develop strategies to keep track of a stable deformation branch during the optimization process. A surprising outcome is that our approach naturally leads to self-emerging bistable structures, which is demonstrated by a series of numerical examples. We believe that our new approach would make substantial contribution to computational design of non-rigid origami structures, benefiting applications in origami-inspired solutions for science and engineering.

1. Introduction

The concept of origami is now prevailing in various fields of engineering and science because their special geometries empower normal materials to exhibit extraordinary performance [1–4]. Its applications include deployable structures [5], shape shifting robots [6], adaptive architectures [7], and metamaterials [8]. One advantage of origami-inspired solutions to engineering problems is that they can be manufactured by means of self-assembly and self-organization, actuated by smart materials under external stimuli [9–13]. Many methods have been proposed to design origami structures, and they are mainly targeting at the design of rigid origami with pure geometric approaches, assuming that all the panels are rigid [14,15]. However, the rigid origami assumption is unable to capture the actual behavior of physical origami structures, which may involve bending, stretching, and shearing of panels during deformation [16,17]. Therefore, the need to incorporate nonlinear mechanics into origami design procedure is a critical and important research topic.

Multiple methods exist to analyze the nonlinear deformation of non-rigid origami. For instance, using the finite element analysis based on shells or solids, researchers have studied the energy absorption property of a variety of origami structures [18–23]. However, such analyses face issues such as high computational cost, and difficulty to converge [24,25]. Therefore, some researchers neglect the elastic energy of the creases and employ the truss structure for origami structural analysis to maintain a balance between accuracy and computational efficiency [26–28]. However, the truss model only applies to origami with triangular panels, and is not suitable for most origami structures. As a result, rotational hinges (or springs) are added to the triangular truss network using small-strain constitutive models, which is used for simulating the crumpling of paper [29], and modal analysis of origami structures [30]. Tailored formulation is also developed to account for the width of smooth creases that are common in practice [31]. Inspired by the linear truss model with rotational springs, Liu and Paulino put forward the nonlinear bar-and-hinge model and develop corresponding nonlinear mechanics theory of origami structures [16]. Under the joint effort of several researchers, the nonlinear bar-and-hinge model is now capable of detecting contact, modeling curved creases, and is still under active development [32,33]. The associated software MERLIN and its derivatives have become a popular tool for nonlinear analysis of non-rigid origami [34].

Computational design of origami has always been a challenging research topic due to its intrinsic complexity [35,36]. Lang develops a Treemaker algorithm for assisting origami artists to find initial bases [37]. Tachi proposes an Origamizer algorithm based on the generalized Ron-Resch pattern, which is later proven to be capable

☆ This paper is part of the Special Issue on Origami Engineering and Physics edited by Edwin A. Peraza Hernandez and Glaucio Paulino.

* Corresponding author.
E-mail address: liuke@pku.edu.cn (K. Liu).

https://doi.org/10.1016/j.mechrescom.2023.104165
Received 7 May 2023; Received in revised form 19 June 2023; Accepted 7 July 2023
Available online 17 July 2023

of folding a piece of paper into any polyhedron [38]. Based on the generalized Miura-ori, Dudte et al. propose an algorithm that enables the fitting of origami patterns onto arbitrary curved surfaces [39]. Upon analyzing the rigid foldability of origami with quadrilateral panels, Dang et al. develop a propagation algorithm that sequentially produces rigid origami patterns with curved shapes [14]. However, all the aforementioned computational design methods are aiming at rigid origami structures, under pure geometric considerations, leaving a gap between the design target and practical applications where the non-rigid behavior of origami is substantial. At present, computational origami design approaches that take into account mechanics factor are still in the early stage of exploration. A pioneering step is taken by casting origami design into a topology optimization framework [40,41], which have been used to design origami actuators, but the creases must be selected from a given finite set of orientations.

In this article, we propose an optimization-based computational design framework, taking into account the nonlinear mechanics of non-rigid origami structures. The proposed formulation yields optimized origami structure with minimized elastic stored energy after a prescribed large deformation. This objective is chosen because of its strong relevance with energy absorption and foldability, which are useful characteristics for applications ranging from morphing structures to cellular materials. A serendipity outcome of this energy minimization formulation is that it creates bistable structures when possible. This phenomenon is explained in detail by our first example in Section 2.

The rest of this paper is structured as follows: Section 2 presents the optimization of a singly corrugated origami structure with one crease, simplified into a two dimensional truss with rotational springs, which provides a simple demonstrative example to our optimization formulation. Section 3 presents optimization of a singly corrugated origami with three creases, adding the complexity of bifurcation. We develop strategies to handle the bifurcation issue so that the optimization is enforced to perform on a stable equilibrium path. In Section 4, we introduce the optimization framework to general origami structures, taking the well-known Miura-ori as an example. Sensitivity analysis of the bar-and-hinge model is also derived. These numerical examples show the potential of our framework to design desired non-rigid origami structures. In these examples it should be noted that we focus on the proportional relationship between different parameters and variables, and thus the physical quantities are dimensionless.

2. Singly corrugated origami with one crease

To illustrate the proposed optimization formulation, we begin with a singly corrugated origami, considering only one folding crease. The structure to be optimized is shown in Fig. 1(a) and (b), which could be simplified into a two dimensional bar-and-hinge model, as shown in Fig. 1(c) and (d). The simplified model involves two elastic bars and one rotational spring. The boundary condition is shown in Fig. 1(c). Owing to symmetry, the middle joint only has one degree of freedom (DOF), which is subject to a downward load of a prescribed displacement $\bar{u}$. For this example, the height of the middle joint is the design variable that determines the configuration of this structure. We aim to obtain the optimal configuration that is of the minimal stored energy after deformation, among all possible configurations.

We first consider a special case when the rotational spring is of zero stiffness, which effectively reduces the structure into a two bar truss. The elastic energy is thus only stored in the bars. Adopting linear elastic constitutive model for the bar elements, we obtain the analytical expression for elastic stored energy of the system as:

$$U_{\text{bar}} = K_{\text{b}}(l_0 - l')^2. \tag{1}$$

In the above equation, U_{bar} is the stored energy of the bar elements, K_{b} is the stiffness of the bar elements, l_0 is the original length of the bar elements, and l' is the length of bar elements after deformation. As the middle joint only moves along the vertical direction, l' could

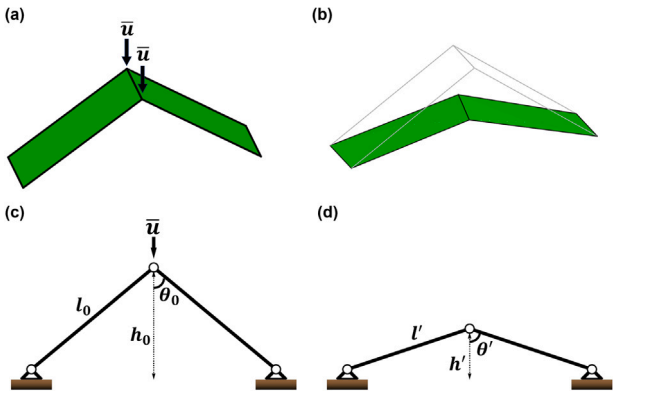

Fig. 1. (a) A singly corrugated origami with one crease, and its boundary conditions. (b) The deformed shape of the origami structure subject to a displacement load $\bar{u}$. (c) A simplified two dimensional bar-and-hinge model for the origami structure in (a). A rotational spring is attached to the middle joint. (d) Deformed shape of the simplified model.

be expressed in terms of l_0 and the original undeformed height of the middle joint (h_0):

$$l' = \sqrt{\bar{u}^2 + l_0^2 - 2\bar{u}h_0}. \tag{2}$$

Substituting the expression for l' into Eq. (1), we can get the analytical expression for the elastic stored energy and its gradient with respect to the design variable h_0:

$$U_{\text{bar}} = K_{\text{b}}(l_0 - \sqrt{\bar{u}^2 + l_0^2 - 2\bar{u}h_0})^2, \tag{3}$$

$$\frac{\partial U_{\text{bar}}}{\partial h_0} = -2K_{\text{b}}\bar{u} + 2K_{\text{b}}l_0\bar{u}\left(\frac{1}{\sqrt{\bar{u}^2 + l_0^2 - 2\bar{u}h_0}}\right). \tag{4}$$

Minimizing the stored energy after deformation, we obtain the analytical solution for the optimal height as $h_0^* = \bar{u}/2$, by solving $\partial U_{\text{bar}}/\partial h_0 = 0$. This optimal structure deforms into its mirror configuration, which releases all the stored energy as the length of bars recovering to their original value. Hence, the minimal stored energy after deformation becomes zero, and the structure becomes bistable.

Next we consider elastic energy stored in both the bars (U_{bar}) and the rotational spring (U_{spr}), to reflect the actual behavior of origami structures. We have the following expression for the total stored energy of the system:

$$U = U_{\text{bar}} + U_{\text{spr}}, \tag{5}$$

where U_{bar} has the same expression with Eq. (3):

$$U_{\text{bar}} = K_{\text{b}}(l_0 - \sqrt{\bar{u}^2 + l_0^2 - 2\bar{u}h_0})^2. \tag{6}$$

Assuming that the rotational spring is linear elastic, the explicit expression for the store energy of the rotational spring is:

$$U_{\text{spr}} = 2K_{\text{spr}}(\theta(h_0) - \theta_0)^2, \tag{7}$$

where K_{spr} is the rotational stiffness of the spring, θ_0 is the original half angle between the two bars before deformation, as a function of h_0 and l_0:

$$\theta_0 = \cos^{-1}\left(\frac{h_0}{l_0}\right). \tag{8}$$

The function $\theta(h_0)$ measures the half angle between the two bars after deformation:

$$\theta(h_0) = \begin{cases} \tan^{-1}\left(\frac{\sqrt{l_0^2 - h_0^2}}{h_0 - \bar{u}}\right) & h_0 \geq \bar{u} \\ \pi - \tan^{-1}\left(\frac{\sqrt{l_0^2 - h_0^2}}{h_0 - \bar{u}}\right) & h_0 < \bar{u} \end{cases} \tag{9}$$

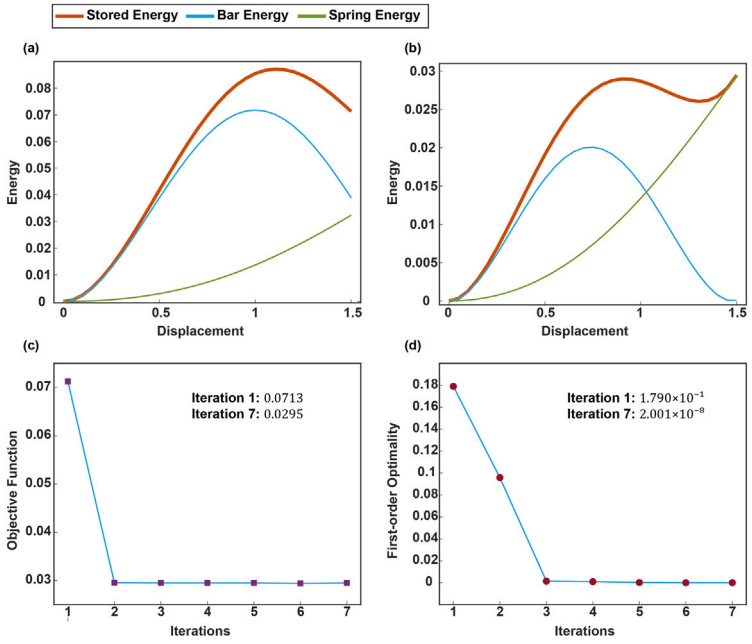

Fig. 2. (a) Energy profile of the unoptimized configuration ($h_0 = 1$) during the deformation process. (b) Energy profile of the optimized configuration ($h_0 = 0.7396$) during the deformation process. We use different colors to draw separately the contribution of energy from bars and rotational spring. (c) Convergence of the objective function. (d) Convergence of the first-order optimality criterion.

The optimization formulation in terms of design variable h_0 is given as follows:

$$\min_{h_0} \quad U(h_0)$$
$$\text{s.t.} \quad 0 \le h_0 \le l_0 \tag{10}$$

To perform gradient-based numerical optimization, we conduct sensitivity analysis and obtain:

$$\frac{\partial U}{\partial h_0} = \frac{\partial U_{\text{bar}}}{\partial h_0} + \frac{\partial U_{\text{spr}}}{\partial h_0}, \tag{11}$$

$$\frac{\partial U_{\text{bar}}}{\partial h_0} = -2K_b\bar{u} + 2K_b l_0 \bar{u}\left(\frac{1}{\sqrt{\bar{u}^2 + l_0^2 - 2\bar{u}h_0}}\right), \tag{12}$$

$$\frac{\partial U_{\text{spr}}}{\partial h_0} = \frac{4}{\sqrt{l_0^2 - h_0^2}}\left(\frac{\bar{u}^2 - h_0\bar{u}}{\bar{u}^2 + l_0^2 - 2\bar{u}h_0}\right)K_{\text{spr}}(\theta(h_0) - \cos^{-1}\left(\frac{h_0}{l_0}\right)) \tag{13}$$

For numerical optimization, we set the structural parameters as $l_0 = 2, K_b = 1, K_{\text{spr}} = 0.025$, and apply a prescribed displacement $\bar{u} = 1.5$. The built-in interior-point algorithm of MATLAB "fmincon" function is employed to perform the optimization. The unoptimized value of h_0 is 1.0, and the optimized height h_0^* is 0.7396, resulting in a significant drop of stored energy under the given displacement load, as shown in Fig. 2(a) and (b). We also note that as the rotational spring is added, although the optimized stored energy after deformation is no longer zero, bistability still emerges at the end of the optimization. The optimized structure deforms into a nearly symmetric configuration after deformation. The energy stored in bars is released as they deform back to original lengths. While the stored energy of the rotational spring continues to increase due to the growing angle, leading to a metastable state with non-zero energy (Fig. 2(b)). The convergence history of the numerical optimization is plotted in Fig. 2(c) and (d).

3. Singly corrugated origami with three creases

3.1. Basic description

From the previous discussion on the one-crease case, we move on to apply the same optimization formulation to a singly corrugated origami structure with three creases, as shown in Fig. 3(a). This example is to demonstrate how to perform origami shape optimization under bifurcation. We propose a material parameter adjusting strategy that allows us to keep track of a stable bifurcation branch and perform structural optimization on it, which is a significant contribution of this article. We investigate this problem with a simplified two dimensional bar-and-hinge model. To be more specific, this structure comprises of three rotational springs and four bars in a symmetric layout, as shown in Fig. 3(c).

Because the structure and boundary condition are both symmetric, we may consider only half DOFs of the structure. We denote the undeformed lengths of the bars as l_1 and l_2, and the lengths after deformation are denoted as l_1' and l_2'. We use intersection angles θ_{10}, θ_{20} to denote the neutral angles of rotational springs at stress-free state, and θ_1, θ_2 stand for the angles after deformation, as shown in Fig. 3. In this example, we set $l_1 = l_2 = 8$, $\theta_{10} = 0.5236$ rad, $\theta_{20} = 0.6236$ rad for numerical evaluations. The vertical displacement load applied at Joint 2 is $\bar{u} = 22$.

The stored energy of this system (U) could be divided into three parts: energy stored in bars: U_{bar}, energy stored in 2 symmetric rotational springs (U_{spr1}), energy stored in the middle rotational spring (U_{spr2}), which leads to:

$$U = U_{\text{bar}} + U_{\text{spr1}} + U_{\text{spr2}}. \tag{14}$$

We denote the stiffness of the two bars as K_{b1} and K_{b2}. The energy stored in the bar elements is expressed as follows:

$$U_{\text{bar}} = K_{\text{b1}}(l_1' - l_1)^2 + K_{\text{b2}}(l_2' - l_2)^2 \tag{15}$$

We denote the rotational stiffness of the spring in Joint 1 and Joint 2 as K_{spr1} and K_{spr2}, respectively. So the expressions for the energy stored in the rotational springs are given by:

$$\begin{aligned} U_{\text{spr1}} &= K_{\text{spr1}}(\theta_1 - \theta_{10} - \theta_2 + \theta_{20})^2 \\ U_{\text{spr2}} &= 2K_{\text{spr2}}(\theta_2 - \theta_{20})^2 \end{aligned} \tag{16}$$

As we take the values of the intersection angles $(\theta_{10}, \theta_{20})$ before deformation as design variables, our optimization problem is formulated as:

$$\min_{\theta_{10},\theta_{20}} \quad U$$

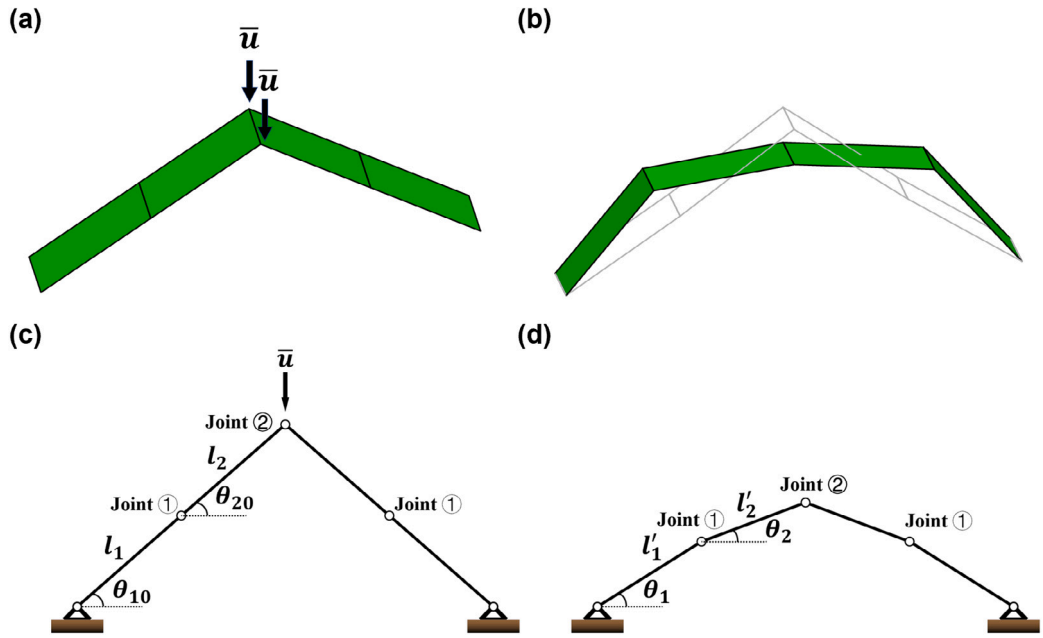

Fig. 3. (a) A singly corrugated origami with three creases, and its boundary conditions. (b) The deformed shape of the origami structure subject to a displacement load $\bar{u}$. (c) A simplified two dimensional bar-and-hinge model for the origami structure in (a), each joint is attached with a rotational spring. (d) Deformed shape of the simplified model.

$$\text{s.t.}\begin{cases} |\theta_{10}| < \pi/2 \\ |\theta_{20}| < \pi/2 \\ l_1(1+\sin\theta_{10}) + l_2(1+\sin\theta_{20}) > \bar{u} \end{cases} \tag{17}$$

We analytically derive the gradient of the objective function. In our problem, the objective function used to optimize the structure is in the following form, in which $\boldsymbol{\theta_0} = [\theta_{10}, \theta_{20}]$ is the vector of design variables:

$$U = f(\boldsymbol{\theta}(\boldsymbol{\theta_0}), \boldsymbol{\theta_0}). \tag{18}$$

This function depends on both the configuration of the deformed structure and the undeformed structure defined by the design variables. Thus its gradient with respect to the design variables is given by:

$$\frac{dU}{d\boldsymbol{\theta_0}} = \frac{\partial U}{\partial \boldsymbol{\theta_0}} + \frac{\partial U}{\partial \boldsymbol{\theta}}\frac{\partial \boldsymbol{\theta}}{\partial \boldsymbol{\theta_0}}, \tag{19}$$

where $\partial U/\partial \boldsymbol{\theta_0}$ and $\partial U/\partial \boldsymbol{\theta}$ are terms generally easy to be derived knowing the analytical expression of U. However, the term $\partial \boldsymbol{\theta}/\partial \boldsymbol{\theta_0}$ shows an implicit dependency that is difficult to obtain. Assuming an elastic system, we use the principle of stationary potential energy to derive the equilibrium condition. The total potential energy Π of the system comprises of two components:

$$\Pi(\mathbf{u}) = U(\mathbf{u}) - V(\mathbf{u}), \tag{20}$$

where U is the system's stored energy and V is the external work. The equilibrium of the system is reached when the potential energy is stationary:

$$\frac{\partial \Pi}{\partial \mathbf{u}} = 0, \tag{21}$$

where $\mathbf{u}$ denotes the free nodal displacements of Joint 1. Differentiation of Eq. (21) with respect to $\boldsymbol{\theta_0}$ is given by:

$$\frac{\partial^2 \Pi}{\partial \mathbf{u}\partial \boldsymbol{\theta_0}} + \frac{\partial^2 \Pi}{\partial \mathbf{u}\partial \boldsymbol{\theta}}\frac{\partial \boldsymbol{\theta}}{\partial \boldsymbol{\theta_0}} = 0. \tag{22}$$

Because $\mathbf{u}$ and $\boldsymbol{\theta}$ has one to one correspondence, the solution of Eq. (21) completely determines the deformed configuration of the structure. We can solve for the value of $\partial \boldsymbol{\theta}/\partial \boldsymbol{\theta_0}$ as follows:

$$\frac{\partial \boldsymbol{\theta}}{\partial \boldsymbol{\theta_0}} = -\left(\frac{\partial^2 \Pi}{\partial \boldsymbol{\theta}\partial \mathbf{u}}\right)^{-1}\frac{\partial^2 \Pi}{\partial \boldsymbol{\theta_0}\partial \mathbf{u}}, \tag{23}$$

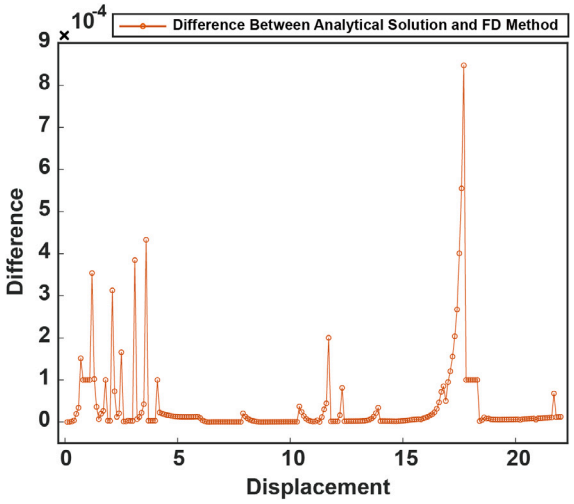

Fig. 4. The difference between the analytical expression and FD approximation versus applied displacement for the three-crease structure in Fig. 3.

where,

$$\frac{\partial^2 \Pi}{\partial \boldsymbol{\theta}\partial \mathbf{u}} = \frac{\partial^2 \Pi}{\partial \mathbf{u}^2}\frac{d\mathbf{u}}{d\boldsymbol{\theta}}. \tag{24}$$

Substituting the value of $\partial \boldsymbol{\theta}/\partial \boldsymbol{\theta_0}$ into Eq. (19), we can obtain the analytical solution for the gradient:

$$\frac{dU}{d\boldsymbol{\theta_0}} = \frac{\partial U}{\partial \boldsymbol{\theta_0}} - \frac{\partial U}{\partial \boldsymbol{\theta}}\left(\frac{\partial^2 \Pi}{\partial \boldsymbol{\theta}\partial \mathbf{u}}\right)^{-1}\frac{\partial^2 \Pi}{\partial \boldsymbol{\theta_0}\partial \mathbf{u}}. \tag{25}$$

The correctness of the derived terms are verified by the finite difference (FD) method as shown in Fig. 4, we apply a displacement to the structure and compare the analytical value with the FD value of the gradient during the deformation. The central difference formula with a step size of 10^{-3} is adopted. The entries of the gradient vector are approximated one by one. The average difference between the analytical expression and the FD approximate is 3.5668×10^{-5}. In general, the two approaches yield almost identical results.

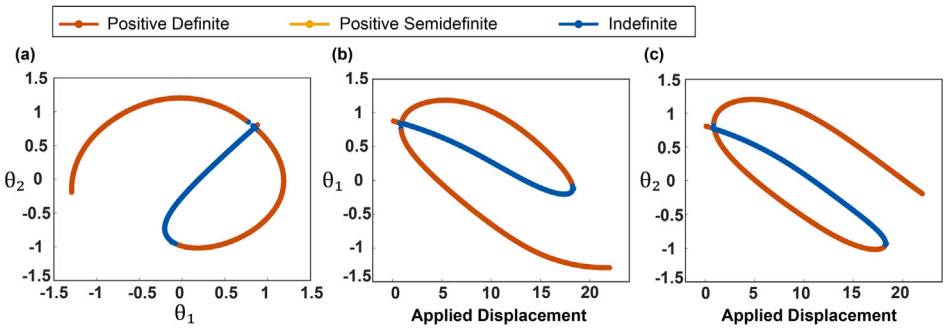

Fig. 5. (a) The bifurcation diagram of the system. (b) The branches of the first structural parameter(θ_1) with respect to the applied displacement load. (c) The branches of the second structural parameter(θ_2) with respect to the applied displacement load.

3.2. Bifurcation analysis

The large deformation of origami that we are dealing with is highly nonlinear, and thus the phenomenon of bifurcation may occur. In other words, there are more than one feasible solutions to Eq. (21), but not all feasible solutions are stable, i.e., at strict energy minimum. The stability of a solution can be examined by checking the signs of the eigenvalues of the Hessian matrix of the total potential energy expression, i.e., the tangent stiffness matrix. If the tangent stiffness matrix is positive definite, then the corresponding equilibrium state is stable; if the tangent stiffness matrix is indefinite, then the corresponding equilibrium state is unstable; if the tangent stiffness matrix is semidefinite, the corresponding equilibrium state may be a state that bifurcation would occur [42]. We plot the equilibrium paths and bifurcation diagram of the system in Fig. 5. We observe that several feasible branches stem out from the critical point, yet not all of them are in stable equilibrium. Typically, the unstable branches are those with higher stored energy.

3.3. Strategies to overcome the bifurcation induced issues

As we have discussed in Section 3.2, different bifurcation branches corresponds to different paths of deformations (as shown in Fig. 6) and some may lead the optimizer to find unfavored solutions. When the optimizer finds an optimal solution by tracing an unstable equilibrium path, the corresponding configuration cannot maintain its shape physically. Meanwhile, these unstable branches normally terminate before reaching final configuration under prescribed displacement load. Hence the optimal configuration may suddenly change during the optimization after termination of these branches, which may leads to fail of convergence. Therefore, it is critical to develop efficient strategies that can keep track of the equilibrium path, and lead the path to stable and desired branches, avoiding sudden switch between different bifurcation branches.

We propose a method by adjustment of material parameters to control bifurcation branches. The method is developed based on the discovery of relationship between the material parameters and the numbers of bifurcation branches. We find that the increase of K_{spr2} makes some bifurcation branches vanish. In particular, the vanished branches are the unstable branches and branches with higher stored energy. Moreover, decrease of K_{b} have a similar effect to reduce the number of unstable branches. This discovery is demonstrated by examples in Fig. 7.

On the basis of the aforementioned method, we develop a multi-stage optimization strategy. Specifically, we perform the optimization in a multi-stage manner, by gradually increasing K_b and decreasing K_{spr2} at consecutive stages. The optimized design at each stage is used as the unoptimized initial design for the next stage of optimization. The parameter adjustment rules between stages are given by:

$$\begin{aligned} &K_{\text{b}}^{k} = K_{\text{b}}^{ini} + \frac{K_{\text{b}}^{fin} - K_{\text{b}}^{ini}}{M^3} k^3, \\ &\text{with} \quad K_{\text{b}}^{ini} = 1.2, K_{\text{b}}^{fin} = 1.8; \\ &K_{\text{spr2}}^{k} = K_{\text{spr2}}^{ini} + \frac{K_{\text{spr2}}^{fin} - K_{\text{spr2}}^{ini}}{M^3} k^3, \\ &\text{with} \quad K_{\text{spr2}}^{ini} = 0.8, K_{\text{spr2}}^{fin} = 0.3. \end{aligned} \tag{26}$$

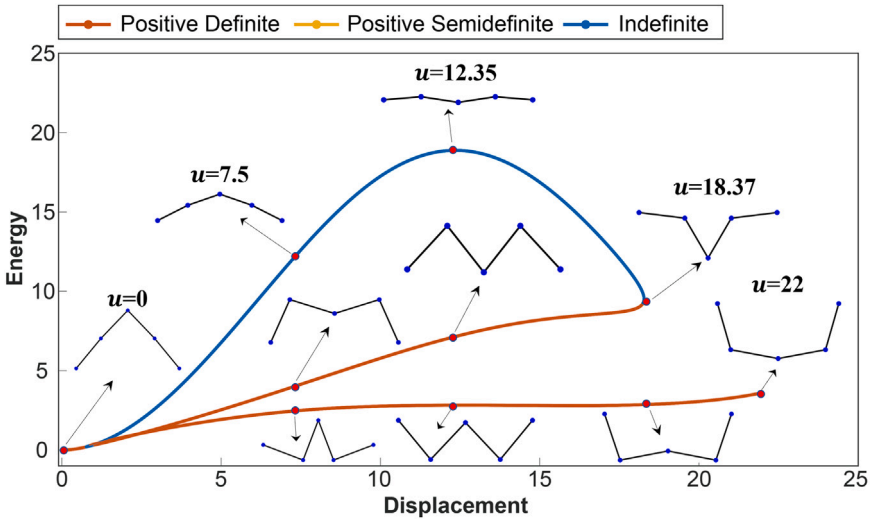

Fig. 6. Difference equilibrium paths of a typical three-crease origami structures and their corresponding configurations. For comparison, we investigate configurations of different branches at $\bar{u} = 0$ (undeformed configuration), $\bar{u} = 7.5$, $\bar{u} = 12.35$ (energy peak of the unstable branch), $\bar{u} = 18.37$ (termination of two branches), and $\bar{u} = 22$ (final configuration).

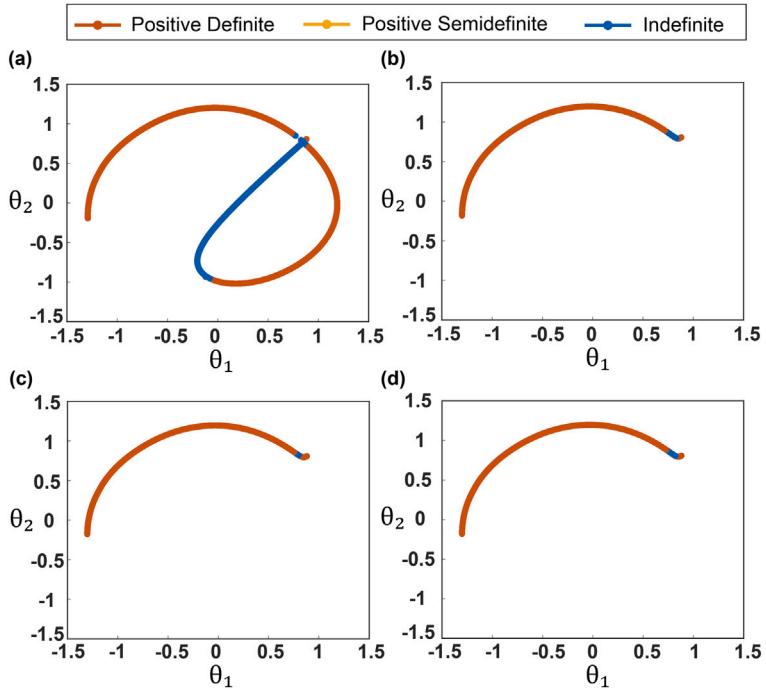

Fig. 7. (a) The bifurcation diagram of the three-crease origami structure when $K_b = 1.2162, K_{spr2} = 0.7865$. (b) The bifurcation diagram of the structure when $K_b = 1.2162, K_{spr2} = 0.8865$. (c) The bifurcation diagram of the structure when $K_b = 1.0162, K_{spr2} = 0.7865$. (d) The bifurcation diagram of the structure when $K_b = 1.1162, K_{spr2} = 0.8365$.

In the above equation, M denotes the total number of adjustment, and $k+1$ is the current number of optimization. For this example, $M = 10$. We also adjust the criteria of convergence at each stage, including optimality tolerance (δ_{opt}) and step-size tolerance (δ_{step}). This is to avoid wasting too much computational effort on early stages that do not produce final result that we are looking for. The adjustment scheme of convergence criteria is given as below:

$$\begin{aligned} &\delta_{step}^{k} = \delta_{step}^{ini} + \frac{\delta_{step}^{fin} - \delta_{step}^{ini}}{M^3} k^3 \\ &\text{with} \quad \delta_{step}^{ini} = 10^{-3}, \delta_{step}^{fin} = 10^{-10} \\ &\delta_{opt}^{k} = \delta_{opt}^{ini} + \frac{\delta_{opt}^{fin} - \delta_{opt}^{ini}}{M^3} k^3 \\ &\text{with} \quad \delta_{opt}^{ini} = 10^{-3}, \delta_{opt}^{fin} = 10^{-6} \end{aligned} \tag{27}$$

In addition to the aforementioned strategy, we propose a heuristic algorithm to limit the step size at each optimization update, to avoid drastic changes of candidate designs between steps that may be associated with different equilibrium paths. The step size constraint at each update is given by:

$$\begin{cases} |\theta_{10}^{i} - \theta_{10}^{i+1}| \le \frac{|\theta_{10}^{i+1} - \theta_{10}^{0}|}{N+(i+1)}, \\ |\theta_{20}^{i} - \theta_{20}^{i+1}| \le \frac{|\theta_{20}^{i+1} - \theta_{20}^{0}|}{N+(i+1)}. \end{cases} \tag{28}$$

In the above equation, the superscripts refer to the iteration number during optimization. The letter N denotes the prescribed maximal number of iteration during each optimization stage.

Using the above strategies, we optimize the structure for $K_b = 1.8$ and $K_{spr2} = 0.3$, starting from $K_b = 1.2$ and $K_{spr2} = 0.8$. By Eq. (26), we obtain a set of material parameters for the multi-stage optimization:

(1) $K_b = 1.2000, K_{spr2} = 0.8000$;
(2) $K_b = 1.2006, K_{spr2} = 0.7995$;
(3) $K_b = 1.2046, K_{spr2} = 0.7960$;
(4) $K_b = 1.2162, K_{spr2} = 0.7865$;
(5) $K_b = 1.2384, K_{spr2} = 0.7680$;
(6) $K_b = 1.2750, K_{spr2} = 0.7375$;
(7) $K_b = 1.3296, K_{spr2} = 0.6920$;
(8) $K_b = 1.4058, K_{spr2} = 0.6285$;
(9) $K_b = 1.5072, K_{spr2} = 0.5440$;
(10) $K_b = 1.6374, K_{spr2} = 0.4355$;
(11) $K_b = 1.8000, K_{spr2} = 0.3000$.

Before performing the multi-stage shape optimization, for all sets of material parameters in the above list, we perform nonlinear analyses to inspect the energy-displacement curves given the applied displacement load for the same the unoptimized configuration (Fig. 8). Snapping behavior is observed when the equilibrium path suddenly jumps from one to another, especially when K_b is large and K_{spr2} is small, yet those are the cases that we are interested. Hence, if we directly optimize for $K_b = 1.8$ and $K_{spr2} = 0.3$, the optimization may fail to converge because different equilibrium paths gives different feedback on sensitivity, and jumping between different paths could confuse the optimizer. We also note that the stored energy of the unoptimized structure is quite high after deformation under the prescribed displacement load.

Then we perform the multi-stage optimization, using the final design from previous stage as the starting point for the next stage. We plot the energy-displacement curve of the optimized structure at each stage in Fig. 9. Compared to the unoptimized structures, the optimized ones all follow stable equilibrium paths without jumping between different branches. We stress that the final stored energy is also much lower than that of the unoptimized structures in Fig. 8. Along the multi-stage optimization, the optimal value of the objective function decreases as we adjusting the material parameters. The final optimized design after the multi-stage optimization evolves to present a clear kink at Joint 1, which breaks the symmetry of Joint 1 and orients the structure to stay on a stable equilibrium path with the lowest energy profile. Moreover, the optimized structure from the last stage is bistable.

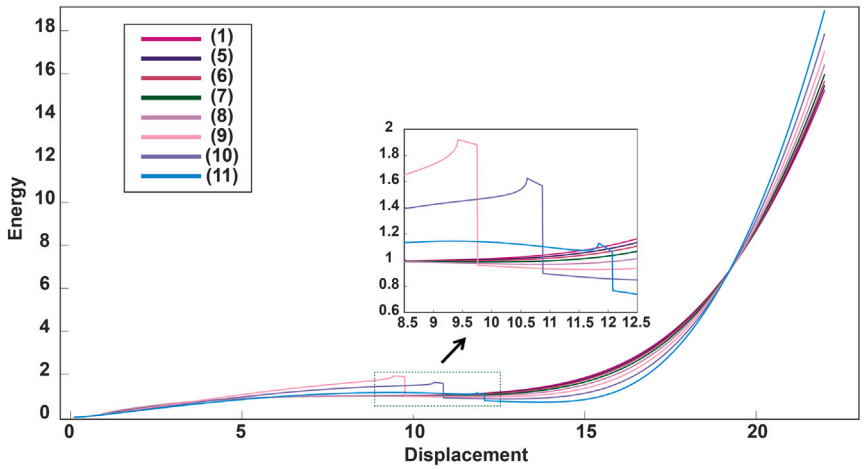

Fig. 8. The energy profiles of the three-crease structure. The configurations are the same, defined by the following design variables: $\theta_{10} = 0.5236, \theta_{20} = 0.6236$. Because the difference between parameters during the early adjustment stages is tiny, the energy profiles cannot be distinguished. So among all sets of material parameters in the above list, we select the set (1) and set (5)-set (11) to plot the energy-displacement curves for the clarity.

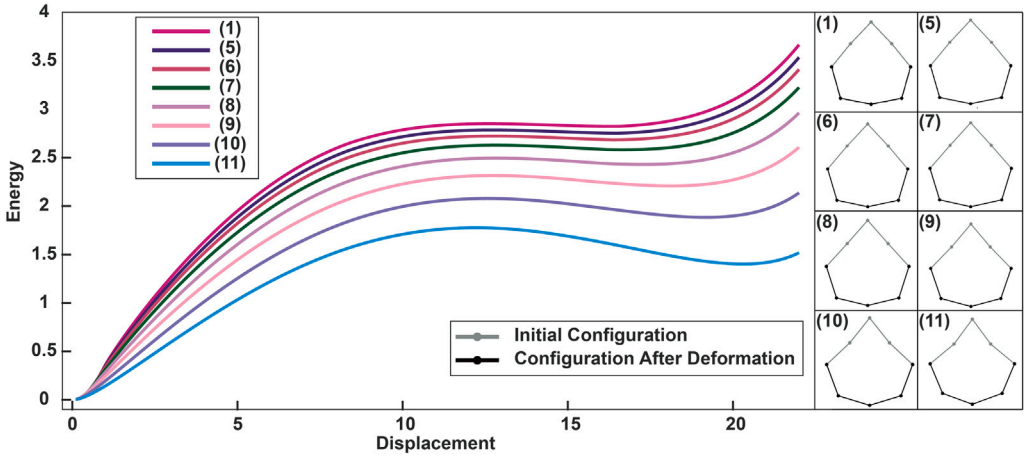

Fig. 9. The energy profiles under different sets of parameters along the process of parameter adjustment. Insets on the right show the optimized structures before and after deformation for different material parameters: set (1) and sets (5) to (11).

4. General origami patterns

4.1. Basic description

For the nonlinear analysis of general origami patterns, we adopt the nonlinear bar-and-hinge model [16] for its versatility and efficiency. This model captures the three essential deformation modes of origami structures: crease folding, panel bending, and panel stretching. The potential energy(Π) of the system comprises of internal strain energy and external work (V_{ext}). We separate the strain energy into two components: one stored in the bar elements (U_{bar}) and the other stored in the rotational springs (U_{spr}). Thus we have the following expression for the total potential energy and the total elastic stored energy:

$$\Pi = U_{\text{bar}} + U_{\text{spr}} - V_{\text{ext}} \tag{29}$$

The stored energy of the ith bar elements is given by:

$$U_{bari} = A^{(i)} L_0^{(i)} W(\lambda), \tag{30}$$

where $A^{(i)}$ is the area of the ith bar, $L_0^{(i)}$ is the undeformed length of the ith bar, W is the strain energy density function, and λ is the one-dimensional stretch of each bar element. We adopt the hyperelastic constitutive law for the strain energy density function as reported in Ref. [16]. For each rotational hinge that represents either a folding crease or bending diagonal of a panel, we define:

$$U_{sprj} = \psi(\theta^{(j)}, K), \tag{31}$$

where ψ is the constitutive law, $\theta^{(j)}$ is the rotation angle of the jth rotational spring, and K is the rotational modulus per unit length along the rotation axis. We define ψ following the original model as in Ref. [16]. Both the bending and folding of origami structures are treated using the same rotational spring constitutive model with different rotational moduli, denoted respectively as K_{b} or K_{f}. Because the stretches (λ) and rotation angles (θ) are completely defined by the nodal displacements ($\mathbf{u}$) and initial nodal positions ($\mathbf{x}_0$), the total stored energy is only a function of $\mathbf{u}$ and $\mathbf{x}_0$.

In our optimization framework, we take the undeformed initial nodal coordinates of the origami structures as design variables. As in the previous examples, the origami structure is optimized subject to prescribed displacement load to minimize the stored energy after deformation. We consider the following nested formulation for the optimization problem:

$$\begin{aligned} &\min_{\mathbf{x_0}} U = \sum_{i=1}^{N_1} U_{\text{bari}}(\mathbf{u}, \mathbf{x_0}) + \sum_{j=1}^{N_2} U_{\text{sprj}}(\mathbf{u}, \mathbf{x_0}) \\ &\text{s.t.}: \quad \mathbf{h}(\mathbf{x_0}) = \mathbf{0} \\ &\text{with}: \quad \partial \Pi(\mathbf{u}, \mathbf{x_0})/\partial \mathbf{u} = \mathbf{0}. \end{aligned} \tag{32}$$

In the objective, $\mathbf{x_0}$ is the nodal coordinates of the undeformed origami structure, $\mathbf{u}$ is the nodal displacements after deformation. The symbols N_1 and N_2 represent the number of bar elements and the number of spring elements, respectively. The term U is the total stored energy of the structure, U_{bari} is the stored energy of the ith bar element, U_{sprj} is the stored energy of the jth spring element. The constraint equation represents generic geometric constraints, such as the Kawasaki condition for flat-foldability, or the developability condition. The state equation in Eq. (32) requires stationary condition of the total potential energy, equivalent to the equilibrium of the system, which is solved by the MERLIN software [16,43].

4.2. Sensitivity analysis

Using the adjoint method to derive the gradient of the elastic stored energy with respect to the undeformed configuration [44,45], we obtain the following expression:

$$\frac{dU}{d\mathbf{x}_0} = \frac{\partial U}{\partial \mathbf{x}_0} - \mathbf{u}^T \left(\frac{\partial^2 U}{\partial \mathbf{x}_0 \partial \mathbf{u}} \right) \tag{33}$$

Taking into account the bar-and-hinge model, we can get the following expanded expression for Eq. (33):

$$\frac{dU}{d\mathbf{x}_0} = \frac{\partial U_{bar}}{\partial \mathbf{x}_0} + \frac{\partial U_{spr}}{\partial \mathbf{x}_0} - \mathbf{u}^T \left(\frac{\partial^2 U_{bar}}{\partial \mathbf{x}_0 \partial \mathbf{u}} + \frac{\partial^2 U_{spr}}{\partial \mathbf{x}_0 \partial \mathbf{u}} \right). \tag{34}$$

Each bar or spring element contributes to Eq. (34) in the following way:

$$\begin{aligned} \frac{\partial U_{sprj}}{\partial \mathbf{x}_0} &= \frac{\partial U_{sprj}}{\partial L_0^{(j)}} \frac{d L_0^{(j)}}{d \mathbf{x}_0} + M^{(j)} \left(\frac{\partial \theta^{(j)}}{\partial \mathbf{x}} - \frac{\partial \theta_0^{(j)}}{\partial \mathbf{x}_0} \right) \\ \frac{\partial U_{bari}}{\partial \mathbf{x}_0} &= \left(W - \lambda \frac{\partial W}{\partial \lambda} \right) A^{(i)} \frac{d L_0^{(i)}}{d \mathbf{x}_0} + A^{(i)} \frac{\partial W}{\partial \lambda} \frac{d L^{(i)}}{d \mathbf{x}} \end{aligned} \tag{35}$$

In the above equations, $L_0^{(i)}$ is the undeformed length of the ith bar, $L^{(i)}$ is bar's length after deformation. The symbol $A^{(i)}$ denotes the area of the ith bar. Similarly, $L_0^{(j)}$ is the undeformed length of the jth rotational hinge, $\theta_0^{(j)}$ is the undeformed rotation angle of the jth rotational hinge, and $\theta^{(j)}$ is the rotation angle after deformation. The symbol $M^{(j)}$ denotes the moment generated by the ith rotational hinge. The principal stretch of a bar element is denoted as λ, and W refers to the energy density function. These definitions follow the same manner as in Ref. [16]. The second order derivatives are given by:

$$\begin{aligned} \frac{\partial^2 U_{sprj}}{\partial \mathbf{u} \partial \mathbf{x}_0} &= \left(\frac{\partial M^{(j)}}{\partial L_0^{(j)}} \frac{d L_0^{(j)}}{d \mathbf{x}_0} - L_0^{(j)} K \frac{\partial \theta_0^{(j)}}{\partial \mathbf{x}_0} \right) \frac{\partial \theta^{(j)}}{\partial \mathbf{x}} + \frac{\partial M^{(j)}}{\partial \theta^{(j)}} \left(\frac{\partial \theta^{(j)}}{\partial \mathbf{x}} \right)^2 + M^{(j)} \frac{\partial^2 \theta^{(j)}}{\partial \mathbf{x}^2}, \\ \frac{\partial^2 U_{bari}}{\partial \mathbf{u} \partial \mathbf{x}_0} &= \frac{A^{(i)}}{L_0^{(i)}} \frac{\partial^2 W}{\partial \lambda^2} \frac{d L^{(i)}}{d \mathbf{x}} \left(-\lambda \frac{d L_0^{(i)}}{d \mathbf{x}_0} + \frac{d L^{(i)}}{d \mathbf{x}} \right) + A^{(i)} \frac{\partial W}{\partial \lambda} \frac{d^2 L^{(i)}}{d \mathbf{x}^2}, \end{aligned} \tag{36}$$

where K is the rotational modulus per unit length along the rotation axis.

4.3. Shape optimization of a miura-ori unit

Among different types of origami structures, the well-known Miura-ori has been extensively used in engineering because of its negative Poisson's ratio and single DOF. Hence, here we choose to optimize the configuration of a Miura-ori unit. We apply a prescribed vertical displacement to the central node (node 5) of a Miura-ori unit. The boundary conditions are shown in Fig. 10. We also apply a constraint for developability such that the angles meet at Node 5 sum to 2π. The interior-point algorithm is adopted as the optimizer.

As shown in Fig. 11, for the unoptimized Miura-ori, the stored energy undergoes sudden drop along the deformation, switching between different bifurcation branches. After the origami structure is optimized, the sudden switch between branches disappears, and the stored energy after deformation decreases significantly. In addition, bistability also

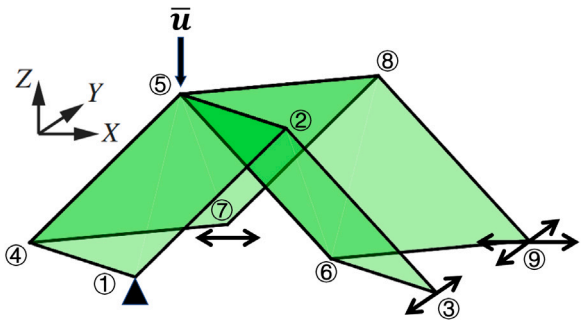

Fig. 10. The Miura-ori unit cell and its boundary conditions. The arrows indicate free DOFs, and the triangles indicate fixed DOFs.

emerges after the optimization in this case, which is clearly seen by the local energy minimum in Fig. 11(b).

To stabilize the optimization process, we adopt the multi-stage optimization strategy by gradually adjusting the structural parameters: the stiffness of the folding creases (K_{f}) and bending creases (K_{b}). This strategy allows us to start the optimization from an origami structure with small number of bifurcation branches, and peform optimization on a stable branch of deformations. Then we gradually decrease the value of K_{b} and increase the value of K_{f}. From Fig. 12, we observe that the energy-displacement curves of the early stages are monotonic, while the curves of later stages display apparent bistable behavior with snap-through (i.e., negative slope on the energy curve). This bistable behavior of the Miura-ori is previously known as the pop-through defect [46]. The energy barrier between the two stable states also increases as we conduct our parameter adjustment strategy.

5. Conclusion

In this paper, we propose a shape optimization framework for the design of non-rigid origami structures. Our optimization framework is developed based on the nonlinear bar-and-hinge model for non-rigid origami structures. The severe nonlinearity of origami deformations leads to bifurcations that hinder the convergence of the optimization. To overcome this critical issue, we develop a multi-stage optimization strategy by gradually adjusting the material parameters of the origami structures. We start demonstrating our idea by elementary examples involving singly corrugated origami structures. We then optimize a Miura-ori unit to show the effectiveness of our design approach for general origami structures. Surprisingly, we discover that our design approach is prone to produce bistable origami designs, which can be very useful for applications in soft robots [47] and metamaterials [48]. Our proposed framework provides new possibilities for incorporating nonlinear mechanics into the design process of origami structures, which is extremely important for engineering applications. Looking forward, this framework may be further improved by adding capabilities such as crease addition and elimination, and composite objective functions for multi-stability.

Declaration of competing interest

The authors declare the following financial interests/personal relationships which may be considered as potential competing interests: Ke Liu reports financial support was provided by Ministry of Industry and Information Technology of the People's Republic of China.

Data availability

Data will be made available on request.

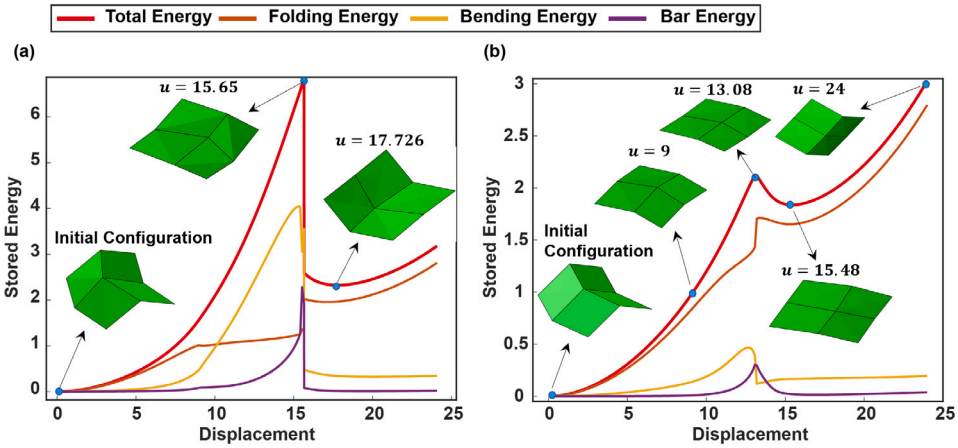

Fig. 11. (a) The energy profile of the Miura-ori unit, for the unoptimized design. (b) The energy profile of the Miura-ori unit for the optimized design. Several snapshots along the deformation process are plotted as insets. The optimal design variables when $K_b = 0.3, K_f = 0.06$ is (24.28,29.30,12.26), and the value of objective function is 3.03. The developability constraint is satisfied up to a deviation of 0.0153.

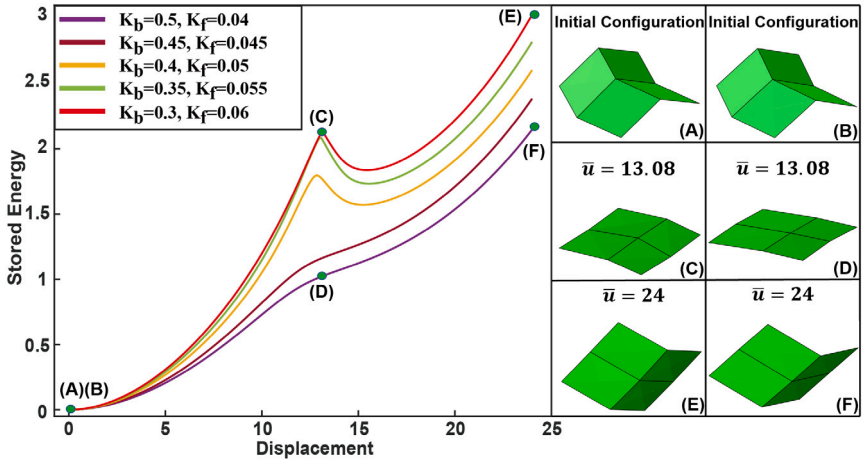

Fig. 12. The energy profiles of the Miura-ori unit at different stages of the multi-stage optimization. The insets show several snapshots along the deformation process for optimized designs with different material parameters. (1): The optimal design variables when $K_b = 0.5, K_f = 0.04$ is (24.20, 29.24, 11.97), and the value of objective function is 2.15. (2): The optimal design variables when $K_b = 0.45, K_f = 0.045$ is (24.03, 29.03, 12.04), and the value of objective function is 2.38. (3): The optimal design variables when $K_b = 0.4, K_f = 0.05$ is (24.29, 29.33, 12.23), and the value of objective function is 2.60. (4): The optimal design variables when $K_b = 0.35, K_f = 0.055$ is (24.30, 29.30, 12.27), and the value of objective function is 2.82. (5): The optimal design variables when $K_b = 0.3, K_f = 0.06$ is (24.28, 29.30, 12.26), and the value of objective function is 3.03.

Acknowledgments

This research is supported by the National Key Research and Development Program of China through grant 2022YFB4701900, and the College of Engineering of Peking University. The authors also thank Dr. Weiwei Wang for helpful discussions during the development of this research.

References

[1] F. Meng, S. Chen, W. Zhang, P. Ou, J. Zhang, C. Chen, J. Song, Negative Poisson's ratio in graphene miura origami, Mech. Mater. 155 (2021) 103774.
[2] S. Waitukaitis, R. Menaut, B.G.-g. Chen, M. van Hecke, Origami multistability: From single vertices to metasheets, Phys. Rev. Lett. 114 (2015) 055503.
[3] E.T. Filipov, G.H. Paulino, T. Tachi, Deployable sandwich surfaces with high out-of-plane stiffness, J. Struct. Eng. 145 (2019) 04018244.
[4] Y. Li, Z. You, Open-section origami beams for energy absorption, Int. J. Mech. Sci. 157–158 (2019) 741–757.
[5] M. Meloni, J. Cai, Q. Zhang, D. Sang-Hoon Lee, M. Li, R. Ma, T.E. Parashkevov, J. Feng, Engineering origami: A comprehensive review of recent applications, design methods, and tools, Adv. Sci. 8 (2021) 2000636.
[6] Q. Chen, F. Feng, P. Lv, H. Duan, Origami spring-inspired shape morphing for flexible robotics, Soft Robotics 9 (2022) 798–806.
[7] P.M. Reis, F. López Jiménez, J. Marthelot, Transforming architectures inspired by origami, Proc. Natl. Acad. Sci. 112 (2015) 12234–12235.
[8] X. Dang, L. Lu, H. Duan, J. Wang, Deployment kinematics of axisymmetric Miura origami: unit cells, tessellations, and stacked metamaterials, Int. J. Mech. Sci. 232 (2022) 107615.
[9] B. An, D. Rus, Programming and controlling self-folding robots, in: 2012 IEEE International Conference on Robotics and Automation, 2012, pp. 3299–3306.
[10] S. Cranford, D. Sen, M.J. Buehler, Meso-origami: Folding multilayer graphene sheets, Appl. Phys. Lett. 95 (2009) 123121.
[11] M. Jamal, S.S. Kadam, R. Xiao, F. Jivan, T.-M. Onn, R. Fernandes, T.D. Nguyen, D.H. Gracias, Bio-origami hydrogel scaffolds composed of photocrosslinked PEG bilayers, Adv. Healthc. Mater. 2 (2013) 1142–1150.
[12] J.-H. Na, A.A. Evans, J. Bae, M.C. Chiappelli, C.D. Santangelo, R.J. Lang, T.C. Hull, R.C. Hayward, Programming reversibly self-folding origami with micropatterned photo-crosslinkable polymer trilayers, Adv. Mater. 27 (2015) 79–85.
[13] S. Felton, M. Tolley, E. Demaine, D. Rus, R. Wood, A method for building self-folding machines, Science 345 (2014) 644–646.
[14] X. Dang, F. Feng, P. Plucinsky, R.D. James, H. Duan, J. Wang, Inverse design of deployable origami structures that approximate a general surface, Int. J. Solids Struct. 234–235 (2022) 111224.
[15] E.D. Demaine, T. Tachi, Origamizer: A practical algorithm for folding any polyhedron, in: 33rd International Symposium on Computational Geometry, SoCG 2017, 2017, pp. 34:1–34:16.
[16] K. Liu, G.H. Paulino, Nonlinear mechanics of non-rigid origami: an efficient computational approach, Proc. R. Soc. Lond. Ser. A Math. Phys. Eng. Sci. 473 (2017) 20170348.
[17] E.T. Filipov, K. Liu, T. Tachi, M. Schenk, G.H. Paulino, Bar and hinge models for scalable analysis of origami, Int. J. Solids Struct. 124 (2017) 26–45.

[18] H. Fang, S.-C.A. Chu, Y. Xia, K.-W. Wang, Programmable self-locking origami mechanical metamaterials, Adv. Mater. 30 (2018) 1706311.
[19] J.M. Gattas, Z. You, The behaviour of curved-crease foldcores under low-velocity impact loads, Int. J. Solids Struct. 53 (2015) 80–91.
[20] Z. Chen, T. Wu, G. Nian, Y. Shan, X. Liang, H. Jiang, S. Qu, Ron resch origami pattern inspired energy absorption structures, J. Appl. Mech. 86 (2019).
[21] L. Yuan, H. Dai, J. Song, J. Ma, Y. Chen, The behavior of a functionally graded origami structure subjected to quasi-static compression, Mater. Des. 189 (2020) 108494.
[22] Z. Liu, W. Hao, Q. Qin, Buckling and energy absorption of novel pre-folded tubes under axial impacts, Appl. Phys. A 123 (2017) 351.
[23] R. Tao, L. Ji, Y. Li, Z. Wan, W. Hu, W. Wu, B. Liao, L. Ma, D. Fang, 4D printed origami metamaterials with tunable compression twist behavior and stress-strain curves, Composites B 201 (2020) 108344.
[24] S. Li, H. Fang, S. Sadeghi, P. Bhovad, K.-W. Wang, Architected origami materials: How folding creates sophisticated mechanical properties, Adv. Mater. 31 (2019) 1805282.
[25] Y. Zhu, M. Schenk, E.T. Filipov, A review on origami simulations: From kinematics, to mechanics, toward multiphysics, Appl. Mech. Rev. 74 (2022) 3.
[26] Z. Zhai, Y. Wang, H. Jiang, Origami-inspired, on-demand deployable and collapsible mechanical metamaterials with tunable stiffness, Proc. Natl. Acad. Sci. 115 (2018) 2032–2037.
[27] C. Jianguo, D. Xiaowei, Z. Ya, F. Jian, T. Yongming, Bistable behavior of the cylindrical origami structure with kresling pattern, J. Mech. Des. 137 (2015).
[28] Y. Wang, X. Zhang, S. Zhu, Highly intensive and controllable supratransmission in a kresling-origami metastructure, Extreme Mech. Lett. 59 (2023) 101964.
[29] A. Lobkovsky, S. Gentges, H. Li, D. Morse, T.A. Witten, Scaling properties of stretching ridges in a crumpled elastic sheet, Science 270 (1995) 1482–1485.
[30] M. Schenk, S.D. Guest, Geometry of miura-folded metamaterials, Proc. Natl. Acad. Sci. 110 (9) (2013) 3276–3281.
[31] E.A. Peraza Hernandez, D.J. Hartl, D.C. Lagoudas, Active Origami: Modeling, Design, and Applications, Springer Cham, 2018.
[32] Y. Zhu, E.T. Filipov, An efficient numerical approach for simulating contact in origami assemblages, Proc. R. Soc. Lond. Ser. A Math. Phys. Eng. Sci. 475 (2230) (2019) 20190366.
[33] S.R. Woodruff, E.T. Filipov, A bar and hinge model formulation for structural analysis of curved-crease origami, Int. J. Solids Struct. 204 (2020) 114–127.
[34] S.W. Grey, F. Scarpa, M. Schenk, Strain reversal in actuated origami structures, Phys. Rev. Lett. 123 (2) (2019) 025501.
[35] E. Demaine, J. O'Rourke, Geometric Folding Algorithms: Linkages, Origami, Polyhedra, Cambridge University Press, 2007.
[36] C.D. Santangelo, Theory and practice of origami in science, Soft Matter 16 (1) (2020) 94–101.
[37] R.J. Lang, The science of origami, Phys. World 20 (2) (2007) 30.
[38] T. Tachi, Origamizing polyhedral surfaces, IEEE Trans. Vis. Comput. Graphics 16 (2010) 298–311.
[39] L.H. Dudte, E. Vouga, T. Tachi, L. Mahadevan, Programming curvature using origami tessellations, Nature Mater. 15 (2016) 583–588.
[40] K. Fuchi, P.R. Buskohl, G. Bazzan, M.F. Durstock, G.W. Reich, R.A. Vaia, J.J. Joo, Origami actuator design and networking through crease topology optimization, J. Mech. Des. 137 (2015).
[41] A.S. Gillman, K. Fuchi, P.R. Buskohl, Discovering sequenced origami folding through nonlinear mechanics and topology optimization, J. Mech. Des. 141 (2019).
[42] N. Boullé, P.E. Farrell, A. Paganini, Control of bifurcation structures using shape optimization, SIAM J. Sci. Comput. 44 (2022) A57–A76.
[43] K. Liu, G. Paulino, Highly efficient nonlinear structural analysis of origami assemblages using the MERLIN2 software, Origami 7 (2018) 1167–1182.
[44] E.D. Sanders, A.S. Ramos, G.H. Paulino, Topology optimization of tension-only cable nets under finite deformations, Struct. Multidiscip. Optim. 62 (2020) 559–579.
[45] C. Groth, A. Chiappa, M.E. Biancolini, Shape optimization using structural adjoint and RBF mesh morphing, Procedia Struct. Integr. 8 (2018) 379–389.
[46] J.L. Silverberg, A.A. Evans, L. McLeod, R.C. Hayward, T. Hull, C.D. Santangelo, I. Cohen, Using origami design principles to fold reprogrammable mechanical metamaterials, Science 345 (6197) (2014) 647–650.
[47] Y. Jiang, Y. Li, K. Liu, H. Zhang, X. Tong, D. Chen, L. Wang, J. Paik, Ultra-tunable bistable structures for universal robotic applications, Cell Rep. Phys. Sci. 4 (2023) 101365.
[48] K. Liu, P.P. Pratapa, D. Misseroni, T. Tachi, G.H. Paulino, Triclinic metamaterials by tristable origami with reprogrammable frustration, Adv. Mater. 34 (43) (2022) 2107998.